COVID

MDPI

Communication

Key Epidemic Parameters of the SIRV Model Determined from Past COVID-19 Mutant Waves

Reinhard Schlickeiser [1,2,*] and Martin Kröger [3,4,*]

[1] Institut für Theoretische Physik, Lehrstuhl IV: Weltraum- und Astrophysik, Ruhr-Universität Bochum, D-44780 Bochum, Germany
[2] Institut für Theoretische Physik und Astrophysik, Christian-Albrechts-Universität zu Kiel, Leibnizstr. 15, D-24118 Kiel, Germany
[3] Magnetism and Interface Physics, Department of Materials, ETH Zurich, CH-8093 Zurich, Switzerland
[4] Polymer Physics, Department of Materials, ETH Zurich, CH-8093 Zurich, Switzerland
* Correspondence: rsch@tp4.rub.de (R.S.); mk@mat.ethz.ch (M.K.)

Abstract: Monitored infection and vaccination rates during past past waves of the coronavirus are used to infer a posteriori two-key parameter of the SIRV epidemic model, namely, the real-time variation in (i) the ratio of recovery to infection rate and (ii) the ratio of vaccination to infection rate. We demonstrate that using the classical SIR model, the ratio between recovery and infection rates tends to overestimate the true ratio, which is of relevance in predicting the dynamics of an epidemic in the presence of vaccinations.

Keywords: coronavirus; statistical analysis; extrapolation; parameter estimation; pandemic spreading

Citation: Schlickeiser, R.; Kröger, M. Key Epidemic Parameters of the SIRV Model Determined from Past COVID-19 Mutant Waves. *COVID* **2023**, *3*, 592–600. https://doi.org/10.3390/covid3040042

Academic Editor: Sandra Costanzo

Received: 17 March 2023
Revised: 6 April 2023
Accepted: 12 April 2023
Published: 13 April 2023

1. Introduction

Massive vaccination campaigns profoundly influence the temporal evolution of pandemic waves. The accurate prediction of the dynamics of epidemics, including quantitatively evaluating the influence of vaccination campaigns, is important to optimize the societal and medical responses to controlling epidemics. The susceptible–infected–recovered/removed–vaccinated (SIRV) epidemic model [1–5] is an important generalization of the simpler susceptible–infected–recovered/removed (SIR) epidemic model originally developed by Kermack and McKendrick [6] and refined by Kendall [7], as the former accounts for the effects of vaccination campaigns on a considered population, while the original SIR model does not take into account vaccinations. Both models are realistic compartment models where persons from the considered population are assigned to the three (SIR) or four (SIRV) compartments: S (susceptible), I (infectious), R (recovered/removed) and (V) vaccinated. The SIR and SIRV epidemic models provide a good explanation for the temporal evolution of COVID-19 waves caused by different mutants [8–10]. Later refinements of these models, such as the SEIR [11–20], SVEIR [21,22], SEIRD [23], SIRD [24–26] and SIRS [27,28], have introduced additional compartments (for reviews, see refs. [29–35]).

Within the SIR and SIRV models, the time-dependent infection ($a(t)$), recovery ($\mu(t)$) and vaccination ($v(t)$) rates regulate the transitions between the compartments $S \to I$, $I \to R$ and $S \to V$. Two important key parameters of the SIRV pandemic model are the ratios $k(t) = \mu(t)/a(t)$ of the recovery to infection rate and $b(t) = v(t)/a(t)$ of the vaccination to infection rate. Recently derived analytical solutions to the SIRV model's equations [1,2] have adopted originally stationary values of the ratios $k(t) = k_0$ and $b(t) = b_0$, allowing for arbitrary time-dependent infection rates $a(t)$. This implies that the recovery and vaccination rates have the same time dependence as the infection rate.

Here, we apply a recently analyzed inversion approach [36] for the SIR model to the SIRV model. Instead of adopting different time dependencies of the rates $k(t)$ and $b(t)$ and then solving the SIRV equations as before, we express key parameters $k(t)$ and $b(t)$ in

terms of the observed rate of new infections $\dot{J}(t)$, its corresponding cumulative fraction $J(t)$ and the known time dependence of the cumulative fraction of vaccinated persons $V(t)$ by using well-monitored data from several countries.

2. SIRV Model

2.1. Starting Equations

The original SIRV equations read as follows:

$$\frac{dS}{dt} = -a(t)SI - v(t)S, \tag{1}$$

$$\frac{dI}{dt} = a(t)SI - \mu(t)I, \tag{2}$$

$$\frac{dR}{dt} = \mu(t)I, \tag{3}$$

$$\frac{dV}{dt} = v(t)S, \tag{4}$$

obeying the sum constraint

$$S(t) + I(t) + R(t) + V(t) = 1 \tag{5}$$

at all times $t \geq t_0$ after the start of the wave at time t_0 with the initial conditions

$$I(t_0) = \eta, \quad S(t_0) = 1 - \eta, \quad R(t_0) = 0, \quad V(t_0) = 0, \tag{6}$$

where η is positive and usually very small, $\eta \ll 1$.

2.2. Key Parameter

In terms of the reduced time

$$\tau = \int_{t_0}^{t} d\xi \, a(\xi), \tag{7}$$

the SIR Equations (1) read as follows:

$$\frac{dS}{d\tau} = -SI - b(\tau)S, \tag{8}$$

$$\frac{dI}{d\tau} = SI - k(\tau)I, \tag{9}$$

$$\frac{dR}{d\tau} = k(\tau)I, \tag{10}$$

$$\frac{dV}{d\tau} = b(\tau)S, \tag{11}$$

with the time-dependent ratios

$$k(\tau(t)) = \frac{\mu(t)}{a(t)}, \qquad b(\tau(t)) = \frac{v(t)}{a(t)}. \tag{12}$$

Combining Equations (8) and (11) yields

$$\frac{d(S+V)}{d\tau} = -SI = -j(\tau) = -\frac{dJ}{d\tau} \tag{13}$$

in terms of the rate of new infections $j(\tau) = SI$ and the cumulative number of new infections $J = \int_0^\tau j(\xi)d\xi$. Equation (13) immediately integrates to

$$J(\tau) = 1 - S(\tau) - V(\tau) = R(\tau) + I(\tau), \tag{14}$$

where the initial conditions (6) determine the integration constant and where the last identity follows from the sum constraint (5).

Combining Equation (8) with Equation (14) provides

$$\begin{aligned} I(\tau) &= -b(\tau) - \frac{dS(\tau)/d\tau}{S(\tau)} = -b(\tau) - \frac{d\ln S(\tau)}{d\tau} \\ &= -b(\tau) - \frac{d}{d\tau}\ln[1 - V(\tau) - J(\tau)]. \end{aligned} \tag{15}$$

For the ratio $b(\tau)$, we use Equation (11) in the form

$$b(\tau) = \frac{1}{S}\frac{dV}{d\tau} = \frac{dV/d\tau}{1 - V - J}, \tag{16}$$

where we inserted S from Equation (14). Combining Equations (15) and (16) then provides

$$I(\tau) = \frac{dJ(\tau)/d\tau}{1 - V(\tau) - J(\tau)} = \frac{j(\tau)}{1 - V(\tau) - J(\tau)}. \tag{17}$$

Likewise, Equation (9) yields

$$k(\tau) = S - \frac{d\ln I}{d\tau} = 1 - V(\tau) - J(\tau) - \frac{d}{d\tau}\ln\left[\frac{j(\tau)}{1 - V(\tau) - J(\tau)}\right], \tag{18}$$

where we used Equations (14) and (17).

Equations (16) and (18) are the first two central results of our investigation. As can be seen the two key parameters b and k can be expressed in terms of the observed epidemic quantities: the rate of new infections j, its cumulative number J and the cumulative number of vaccinated persons V.

2.3. Comparison with the SIR Model Limit

The SIR model corresponds to the limit of no vaccinations $v = b = 0$ corresponding to $V = 0$. At this limit, the general result (18) reduces readily to

$$\begin{aligned} k_{\mathrm{SIR}}(\tau) &= 1 - J(\tau) - \frac{d}{d\tau}\ln\left[\frac{j(\tau)}{1 - J(\tau)}\right] \\ &= 1 - J(\tau) - \frac{d}{d\tau}\ln\left[\frac{d}{d\tau}\ln[1 - J(\tau)]^{-1}\right]. \end{aligned} \tag{19}$$

The derived k_{SIR} agrees exactly with the earlier derived Equation (12) in ref. [36]. The difference

$$\begin{aligned} k_{\mathrm{SIR}}(\tau) - k(\tau) &= V(\tau) + \frac{d}{d\tau}\ln\frac{1 - J(\tau)}{1 - V(\tau) - J(\tau)} \\ &= V(\tau) + \frac{j(\tau)V(\tau) + [1 - J(\tau)]\frac{dV(\tau)}{d\tau}}{[1 - J(\tau)][1 - V(\tau) - J(\tau)]} \geq 0 \end{aligned} \tag{20}$$

is always non-negative because all quantities on the right-hand side of (20) are positive, including the derivative $dV/d\tau$ of the cumulative fraction of vaccinated persons. Consequently, for the same values of $J(\tau)$ and $j(\tau)$, the general ratio k for the SIRV model is always smaller than the ratio k_{SIR} for the SIR model for finite values of $V(\tau)$. This result is very reasonable: to yield an unchanged cumulative number of new infections, compared with the SIR scenario without vaccinations, the value of the ratio k of the SIRV has to be smaller than the k_{SIR}. This inequality is accompanied by a correspondingly higher infection rate.

To shed some light on the obtained results and the difference between k and k_{SIR}, consider a synthetic scenario, where $k(\tau)$ and $b(\tau)$ are given analytically, and the SIRV Equations (8)–(11) are used to calculate the reduced time evolution of the SIRV values. In the next section, we will perform the reverse method and use measured real-time values of $I(t)$ and $V(t)$ to calculate $k(t)$ and $b(t)$. Figure 1 shows the numerical solution of the coupled system of differential SIRV equations for the case of a constant ratio between vaccination and infection rates, $b(\tau)$, and a time-dependent ratio $k(\tau)$ that rises during the course of reduced time τ from 0.3 to 0.8. The initial condition at $\tau = 0$ is given by Equation (6) with a tiny $\eta \ll 1$. The chosen form of $k(\tau)$ is specified in the caption of Figure 1 and plotted in Figure 1c. Figure 1a,b display the solutions of the SIR and SIRV models, respectively. While $V(\tau) = 0$ in the former case, $V(\tau)$ rises monotonously in the latter, giving rise to a significant decrease in the fraction of infected persons. Because vaccination is assumed to be ongoing after the number of infections has dropped, the fraction of susceptible persons continues decreasing towards zero. While $I(\tau)$ denotes the fraction of infected persons at time τ, the quantity $j(\tau)$ is the usually measured differential fraction of infected persons. Figure 1c highlights the difference between $k(\tau)$ and $k_{\mathrm{SIR}}(\tau)$, if both are evaluated using the data shown in Figure 1b. As discussed, $k_{\mathrm{SIR}}(\tau)$ is seen to overestimate $k(\tau)$.

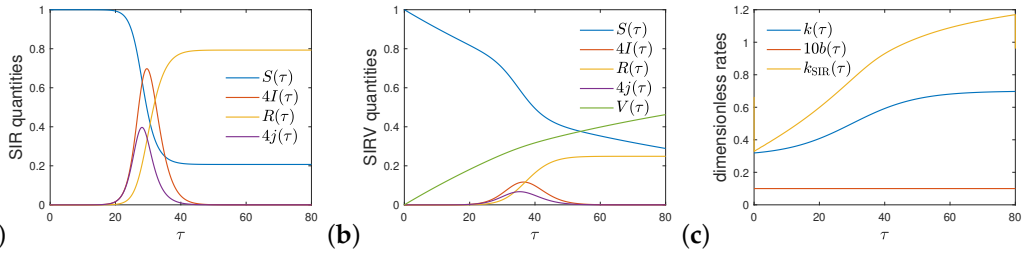

Figure 1. Solution to the (**a**) SIR and (**b**) SIRV models versus reduced time τ for $k(\tau) = 0.5 + 0.2\tanh[0.05(\tau - 30)]$, $\eta = 10^{-8}$ and $b(\tau) = 0$ and $b(\tau) = 0.01$ in (**a**) and (**b**), respectively. Shown are $S(\tau)$, $I(\tau)$, $R(\tau)$, $V(\tau)$ as well as $j(\tau) = S(\tau)I(\tau)$. (**c**) Assuming that the data in (**b**) had been measured, $k(\tau)$ and $b(\tau)$ are correctly reconstructed from Equations (18) and (16). For comparison, we show $k_{\mathrm{SIR}}(\tau)$ obtained from Equation (19). The displayed values of I, j and b were multiplied by factors of 4, 4 and 10, respectively, in order to avoid overlarge figures.

2.4. Real Time Dependence

In terms of the real time dependence, $\dot{J}(t) = a(t)j(\tau)$, $J(t) = J(\tau)$, $V(t) = V(\tau)$ and $\dot{V}(t) = (dV/dt) = a(t)(dV/d\tau)$ are the general ratios, and (16) and (18) read as follows:

$$b(t) = \frac{\dot{V}(t)}{a(t)[1 - V(t) - J(t)]}, \tag{21}$$

$$k(t) = 1 - V(t) - J(t) - \frac{1}{a(t)}\frac{d}{dt}\ln\frac{\dot{J}(t)}{a(t)[1 - V(t) - J(t)]}. \tag{22}$$

Multiplying Equation (21) with $a(t)$ yields $b(t) = v(t)/a(t)$ for the vaccination rate:

$$v(t) = \frac{\dot{V}(t)}{1 - V(t) - J(t)}, \tag{23}$$

which is generally valid at all times t. As in [36], we also consider the case of a stationary infection rate $a(t) = a_0$. In this case, all real-time dependencies of the ratios $k(t)$ and $b(t)$

are attributed to time-dependent recovery ($\mu(t)$) and vaccination ($v(t)$) rates. Equation (22) then reduces to

$$\begin{aligned} b(t) &= \frac{\dot{V}((t)}{a_0[1-V(t)-J(t)]}, \\ k(t) &= 1-V(t)-J(t)-\frac{1}{a_0}\frac{d}{dt}\ln\frac{\dot{J}(t)}{a_0[1-V(t)-J(t)]} \\ &= 1-V(t)-J(t)-\frac{1}{a_0}\left[\frac{\ddot{J}(t)}{\dot{J}(t)}+\frac{\dot{V}(t)+\dot{J}(t)}{1-V(t)-J(t)}\right]. \end{aligned} \tag{24}$$

The difference between $k(t)$ and $k_{\mathrm{SIR}}(t)$ in real time, analogous to (20), is confirmed by Figure 2b, where, for Germany and using $a_0 = 5$ day^{-1} [37], the difference between the values of k is shown, calculated with and without the effect of vaccinations. The sign change of $k(t)$ visible at later times in Figure 2b may be used as an indicator that the sum $J(t)+V(t)$ (Figure 2a) approaches unity, or alternatively, that the mortality ratio $f = D(t)/J(t)$ has significantly changed at the time of the divergence. This time (end of 2021) seems to coincide with the onset of the Omicron wave.

The curves are qualitatively very similar for other countries. In Figure 3a, we report data for the daily number of new fatalities divided by $f = 0.005$ and the size of the population to account for the fatality rate f. This approach allows us to estimate the daily fraction of the population becoming newly infected persons, $\dot{J}(t)$, with much higher accuracy than using the often incomplete reported fraction of newly infected persons. The latter numbers cannot be used due to an unknown number of infections. Using this approach, we follow previous works [37]. Figure 3b shows the corresponding cumulative fraction of infected persons, while Figure 4a,b displays the reported vaccination data for the same eight countries: Australia (AUS), Switzerland (CHE), Germany (DEU), France (FRA), Italy (ITA), Sweden (SWE) and the United States (USA). The dimensionless rates $k(t)$ and $b(t)$ that we obtain using these data in Equation (24) are given in Figure 5. As for Germany, the $k(t)$ decreases with time until the fractions of vaccinated and infected persons approach unity.

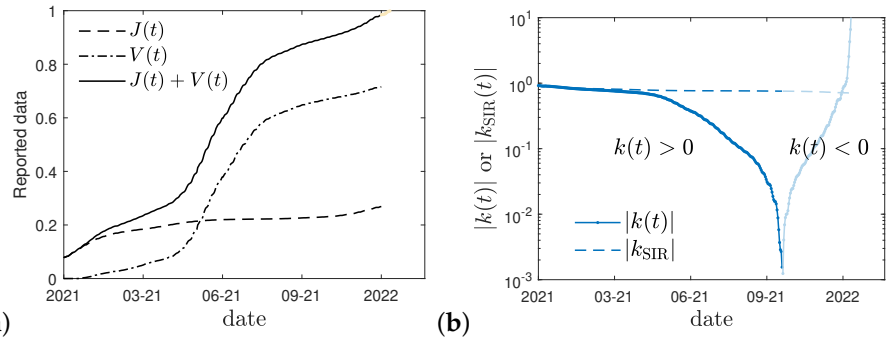

Figure 2. (**a**) Reported data [38] for Germany for the estimated cumulative fraction $I(t) = 200\,D(t)$ of infected people, where $D(t)$ is the reported cumulative fraction of fatalities and $V(t)$is the cumulative fraction of vaccinated persons, as well as their sum. We assume here that vaccinated and infected fractions belong to disjunct compartments, the SIRV model therefore breaks down as soon as the reported $I(t)+V(t)$ exceeds unity, manifested by a sign change of $k(t)$. (**b**) Ratios $k(t)$ (solid) and $k_{\mathrm{SIR}}(t)$ (dashed) according to Equation (24) with and without $V(t)$, respectively.

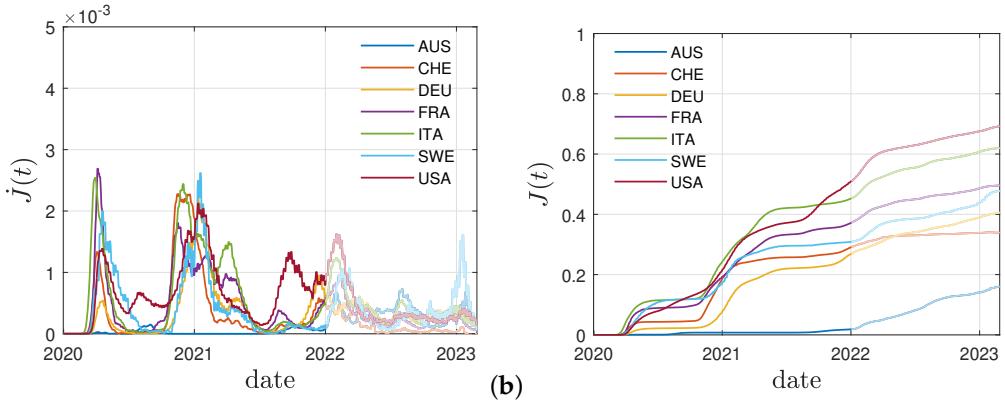

Figure 3. (**a**) Daily fraction $\dot{J}(t)$ and (**b**) cumulative fraction $J(t)$ of infected persons in Australia (AUS), Switzerland (CHE), Germany (DEU), France (FRA), Italy (ITA), Sweden (SWE) and the United States (USA). Up to the end of 2021, the number of truly infected persons is estimated from the number of fatalities, using a fatality rate of 0.005. Afterwards, due to a not precisely known change in the fatality rate, the estimated $\dot{J}(t)$ is not considered in this work. The raw data were retrieved from [38].

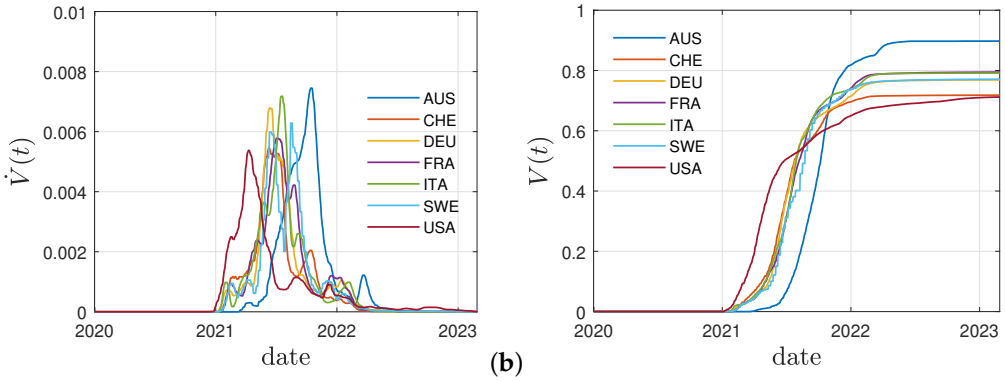

Figure 4. (**a**) Daily fraction and (**b**) cumulative fraction of fully vaccinated persons in Australia (AUS), Switzerland (CHE), Germany (DEU), France (FRA), Italy (ITA), Sweden (SWE) and the United States (USA). The raw data were retrieved from [38].

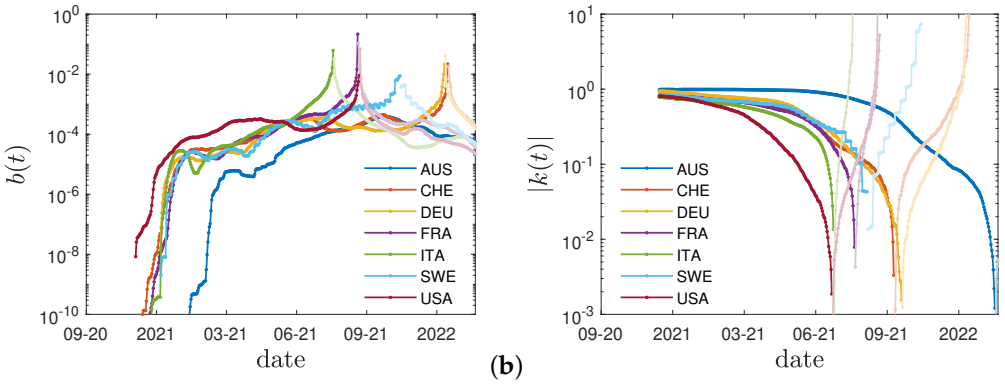

Figure 5. Dimensionless ratios (a) $b(t)$ and (b) $k(t)$ evaluated using Equation (24) and the data shown in Figures 3 and 4. As in Figure 2, regimes with $k(t) < 0$, here also $b(t)$, are indicated by light color. The raw data were retrieved from [38].

3. Cumulative Vaccination Fraction

In Figure 4, the real-time history of the vaccination campaigns in selected countries is shown, indicating the daily fractions of fully vaccinated persons and the total fraction summed over all vaccination campaigns. It can be seen that the shape of the cumulative fraction as a function of real time and their values are of the same order.

The cumulative fraction of total vaccinated persons shown in Figure 4 can be represented well by the function

$$V(t) = V_\infty \left[1 - e^{-\frac{t-t_A}{t_F}}\right] \Theta[t - t_A], \tag{25}$$

where Θ denotes the step function. The parameters V_∞ and t_A, t_F of the function (25) differ for different countries and are listed in Table 1. The starting time of the vaccination campaigns $t_A > t_0$ in general is later than the starting time of the mutant wave t_0.

Table 1. Effective vaccination onset t_A, relaxation time τ and final fraction of fully vaccinated persons V_∞ obtained using Equations (25) and vaccination data shown in Figure 4; t_A is specified in number of days after 1 January 2020.

Country	α_3 Code	t_A	τ	V_∞
Australia	AUS	570	78 days	0.90
Switzerland	CHE	479	86 days	0.72
Germany	DEU	491	83 days	0.76
France	FRA	494	92 days	0.80
Italy	ITA	492	88 days	0.79
Sweden	SWE	503	85 days	0.77
United States	USA	407	122 days	0.70

4. Conclusions

We have derived explicit expressions for the two potentially time-dependent, and dimensionless parameters $k(t)$ and $b(t)$ of the SIRV model in terms of measured and measurable fractions. Obtaining such parameters from reported data is an important prerequisite in the forecasting of the time-evolution of epidemics. The time-evolution of these parameters, which are often considered constant to simplify the analysis, may be better modeled with time-evolutions from past epidemics at hand. To this end, we analyzed their time-dependency and moreover showed that, using the classical SIR model, the ratio between recovery and infection rate, $k(t)$, can be highly overestimated in the presence of vaccinations. We furthermore highlighted the effect of vaccinations on the time-evolution of the $k(t)$ and $b(t)$, which in turn determine the S, I, R and V dynamics in a straightforward fashion.

The proposed inversion method allows one to infer the key parameters of the SIRV pandemic model from past COVID-19 mutant waves in terms of the well-monitored cumulative fractions of new infections and vaccinations. A sign change in the temporal evolution of the ratio between the recovery and infection rate can be used as a diagnostic indicator for a significant change in the mortality ratio of an ongoing mutant wave.

Author Contributions: Conceptualization, R.S.; methodology, R.S. and M.K.; software, M.K.; writing—original draft preparation, R.S.; writing—review and editing, R.S. and M.K.; visualization, M.K. All authors have read and agreed to the published version of the manuscript.

Funding: This research received no external funding.

Informed Consent Statement: Not applicable.

Data Availability Statement: The raw, real-time data used in this study were retrieved from [38].

Conflicts of Interest: The authors declare no conflict of interest.

References

1. Schlickeiser, R.; Kröger, M. Analytical modeling of the temporal evolution of epidemics outbreaks accounting for vaccinations. *Physics* **2021**, *3*, 386–426. [CrossRef]
2. Babaei, N.A.; Ozer, T. On exact integrability of a COVID-19 model: SIRV. *Math. Meth. Appl. Sci.* **2023**, *1*, 1–18. [CrossRef]
3. Rifhat, R.; Teng, Z.; Wang, C. Extinction and persistence of a stochastic SIRV epidemic model with nonlinear incidence rate. *Adv. Diff. Eqs.* **2021**, *2021*, 200. [CrossRef]
4. Ameen, I.; Baleanu, D.; Ali, H.M. An efficient algorithm for solving the fractional optimal control of SIRV epidemic model with a combination of vaccination and treatment. *Chaos Solit. Fract.* **2020**, *137*, 109892. [CrossRef]
5. Oke, M.O.; Ogunmiloro, O.M.; Akinwumi, C.T.; Raji, R.A. Mathematical Modeling and Stability Analysis of a SIRV Epidemic Model with Non-linear Force of Infection and Treatment. *Commun. Math. Appl.* **2019**, *10*, 717–731. [CrossRef]
6. Kermack, W.O.; McKendrick, A.G. A contribution to the mathematical theory of epidemics. *Proc. R. Soc. A* **1927**, *115*, 700. [CrossRef]
7. Kendall, D.G. Deterministic and stochastic epidemics in closed populations. In Proceedings of the Third Berkeley Symposium on Mathematical Statistics and Probability, Berkeley, CA, USA, 1 January 1956; Volume 4, pp. 149–165. [CrossRef]
8. Postnikov, E.B. Estimation of COVID-19 dynamics "on a back-of-envelope": Does the simplest SIR model provide quantitative parameters and predictions? *Chaos Solit. Fract.* **2020**, *135*, 109841. [CrossRef]
9. Cooper, I.; Mondal, A.; Antonopoulos, C.G. A SIR model assumption for the spread of COVID-19 in different communities. *Chaos Solit. Fract.* **2020**, *139*, 110057. [CrossRef]
10. Hespanha, J.P.; Chinchilla, R.; Costa, R.R.; Erdal, M.K.; Yang, G. Forecasting COVID-19 cases based on a parameter-varying stochastic SIR model. *Annu. Rev. Control* **2021**, *51*, 460–476. [CrossRef]
11. Annas, S.; Pratama, M.I.; Rifandi, M.; Sanusi, W.; Side, S. Stability analysis and numerical simulation of SEIR model for pandemic COVID-19 spread in Indonesia. *Chaos Solit. Fract.* **2020**, *139*, 110072. [CrossRef]
12. Hou, C.; Chen, J.; Zhou, Y.; Hua, L.; Yuan, J.; He, S.; Guo, Y.; Zhang, S.; Jia, Q.; Zhao, C.; et al. The effectiveness of quarantine of Wuhan city against the Corona Virus Disease 2019 (COVID-19): A well-mixed SEIR model analysis. *J. Med. Virol.* **2020**, *92*, 841–848. [CrossRef] [PubMed]
13. Yang, Z.; Zeng, Z.; Wang, K.; Wong, S.S.; Liang, W.; Zanin, M.; Liu, P.; Cao, X.; Gao, Z.; Mai, Z.; et al. Modified SEIR and AI prediction of the epidemics trend of COVID-19 in China under public health interventions. *J. Thorac. Dis.* **2020**, *12*, 165. [CrossRef]
14. He, S.; Peng, Y.; Sun, K. SEIR modeling of the COVID-19 and its dynamics. *Nonlin. Dyn.* **2020**, *101*, 1667–1680. [CrossRef] [PubMed]
15. Rezapour, S.; Mohammadi, H.; Samei, M.E. SEIR epidemic model for COVID-19 transmission by Caputo derivative of fractional order. *Adv. Diff. Eqs.* **2020**, *2020*, 490. [CrossRef]
16. Ghostine, R.; Gharamti, M.; Hassrouny, S.; Hoteit, I. An Extended SEIR Model with Vaccination for Forecasting the COVID-19 Pandemic in Saudi Arabia Using an Ensemble Kalman Filter. *Mathematics* **2021**, *9*, 636. [CrossRef]
17. Berger, D.; Herkenhoff, K.; Huang, C.; Mongey, S. Testing and reopening in an SEIR model. *Rev. Econ. Dyn.* **2022**, *43*, 1–21. [CrossRef]
18. Engbert, R.; Rabe, M.M.; Kliegl, R.; Reich, S. Sequential Data Assimilation of the Stochastic SEIR Epidemic Model for Regional COVID-19 Dynamics. *Bull. Math. Biol.* **2021**, *83*, 1. [CrossRef]
19. Bentout, S.; Chen, Y.; Djilali, S. Global Dynamics of an SEIR Model with Two Age Structures and a Nonlinear Incidence. *Acta Appl. Math.* **2021**, *171*, 7. [CrossRef]
20. Carcione, J.M.; Santos, J.E.; Bagaini, C.; Ba, J. A Simulation of a COVID-19 Epidemic Based on a Deterministic SEIR Model. *Front. Publ. Health* **2020**, *8*, 230. [CrossRef]
21. Nabti, A.; Ghanbari, B. Global stability analysis of a fractional SVEIR epidemic model. *Math. Meth. Appl. Sci.* **2021**, *44*, 8577–8597. [CrossRef]
22. Lopez, L.; Rodo, X. A modified SEIR model to predict the COVID-19 outbreak in Spain and Italy: Simulating control scenarios and multi-scale epidemics. *Results Phys.* **2021**, *21*, 103746. [CrossRef]
23. Korolev, I. Identification and estimation of the SEIRD epidemic model for COVID-19. *J. Econom.* **2021**, *220*, 63–85. [CrossRef] [PubMed]
24. Jahanshahi, H.; Munoz-Pacheco, J.M.; Bekiros, S.; Alotaibi, N.D. A fractional-order SIRD model with time-dependent memory indexes for encompassing the multi-fractional characteristics of the COVID-19. *Chaos Solit. Fract.* **2021**, *143*, 110632. [CrossRef] [PubMed]
25. Nisar, K.S.; Ahmad, S.; Ullah, A.; Shah, K.; Alrabaiah, H.; Arfan, M. Mathematical analysis of SIRD model of COVID-19 with Caputo fractional derivative based on real data. *Results Phys.* **2021**, *21*, 103772. [CrossRef]
26. Faruk, O.; Kar, S. A Data Driven Analysis and Forecast of COVID-19 Dynamics during the Third Wave Using SIRD Model in Bangladesh. *Covid* **2021**, *1*, 503–517. [CrossRef]
27. Rajasekar, S.P.; Pitchaimani, M. Ergodic stationary distribution and extinction of a stochastic SIRS epidemic model with logistic growth and nonlinear incidence. *Appl. Math. Comput.* **2020**, *377*, 125143. [CrossRef]
28. Hu, H.; Yuan, X.; Huang, L.; Huang, C. Global dynamics of an SIRS model with demographics and transfer from infectious to susceptible on heterogeneous networks. *Math. Biosci. Eng.* **2019**, *16*, 5729–5749. [CrossRef] [PubMed]

29. Keeling, M.J.; Rohani, P. *Modeling Infectious Diseases in Humans and Animals*; Princeton University Press: Princeton, NJ, USA, 2008. [CrossRef]
30. Estrada, E. COVID-19 and SARS-COV-2, Modeling the present, looking at the future. *Phys. Rep.* **2020**, *869*, 1. [CrossRef]
31. Lopez, L.; Rodo, X. The end of social confinement and COVID-19 re-emergence risk. *Nat. Hum. Behav.* **2020**, *4*, 746–755. [CrossRef] [PubMed]
32. Miller, I.F.; Becker, A.D.; Grenfell, B.T.; Metcalf, C.J.E. Disease and healthcare burden of COVID-19 in the United States. *Nat. Med.* **2020**, *26*, 1212–1217. [CrossRef]
33. Reiner, R.C., Jr.; Barber, R.M.; Collins, J.K.; Zheng, P.; Adolph, C.; Albright, J.; Antony, C.M.; Aravkin, A.Y.; Bachmeier, S.D.; Bang-Jensen, B.; et al. Modeling COVID-19 scenarios for the United States. *Nat. Med.* **2021**, *27*, 94–105. [CrossRef]
34. Linka, K.; Peirlinck, M.; Sahli Costabal, F.; Kuhl, E. Outbreak dynamics of COVID-19 in Europe and the effect of travel restrictions. *Comp. Meth. Biomech. Biomed. Eng.* **2020**, *23*, 710–717. [CrossRef] [PubMed]
35. Filindassi, V.; Pedrini, C.; Sabadini, C.; Duradoni, M.; Guazzini, A. Impact of COVID-19 First Wave on Psychological and Psychosocial Dimensions: A Systematic Review. *Covid* **2022**, *2*, 273–340. [CrossRef]
36. Schlickeiser, R.; Kröger, M. Determination of a key pandemic parameter of the SIR-epidemic model from past COVID-19 mutant waves and its variation for the validity of the Gaussian evolution. *Physics* **2023**, *5*, 205–214. [CrossRef]
37. Schlickeiser, R.; Kröger, M. Reasonable limiting of 7-day incidence per hundred thousand value and herd immunization in Germany and other countries. *Covid* **2021**, *1*, 130–136. [CrossRef]
38. Dong, E.; Du, H.; Gardner, L. An interactive web-based dashboard to track COVID-19 in real time. *Lancet Infect. Dis.* **2020**, *20*, 533–534. Available online: https://pomber.github.io/covid19/timeseries.json (accessed on 5 February 2023). [CrossRef] [PubMed]